Gradient-Based Near-Field Antenna Characterization in Planar Geometry

Amedeo Capozzoli, Claudio Curcio, and Angelo Liseno

Dipartimento di Ingegneria Elettrica e delle Tecnologie dell'Informazione
Università di Napoli Federico II, via Claudio 21, 80125, Napoli, Italia
a.capozzoli@unina.it, clcurcio@unina.it, angelo.liseno@unina.it

Abstract — A near field characterization technique, based on the optimization of the Singular Value Behavior, is here accelerated by using the analytical expression of the gradient of the relevant objective functional. This solution allows to conveniently tackle the cases of electrically large antennas.

Index Terms — Antenna measurements, near field/far field transformation, planar scanning, probe compensation, singular values.

I. INTRODUCTION

The Near-Field (NF) antenna characterization amounts to estimate the Far Field Pattern (FFP) of an Antenna Under Test (AUT), from field data measured in the NF zone [1]. Amplitude and phase or phaseless [2-4] measurements can be exploited; standard metallic or photonic probes can be adopted [5].

In [2-5], the NF characterization has been formulated as a regularized linear inverse problem, outperforming other approaches in terms of number of samples and path length of the scanning curve. The approach has been applied to the canonical scanning geometries in the case of aperture antennas [2-7].

In particular, the number M and the distribution of the field samples (DFS) are determined after a proper optimization procedure improving as much as possible the degree of conditioning of the problem. The procedure is based on the Singular Value (SV) decomposition of the relevant discretized linear operator and on the concept of Singular Value Behavior (SVB) optimization. The DFS and M are determined by means of an iterative process wherein, from one iteration to the next, M is progressively enlarged. At each step, and for a fixed number of samples, the DFS is found as the one optimizing a functional measuring the SVB of the relevant linear operator. The process ends when a saturation behavior of the optimized functional values is observed [2,3]. Given the DFS, the aperture field, and the FFP, can be obtained from the measurements, after a regularized inversion. For electrically large antennas the whole procedure can be accelerated to keep low the computing time required to tackle the optimization.

The crucial steps are:

- Filling the matrix $\underline{\underline{T}}$ representing the discretized version of the linear operator;
- Calculating the SV Decomposition (SVD) of T;
- Optimizing the SVB of T.

As long as a local tool is deemed adequate to optimize the SVB of $\underline{\underline{T}}$, it is convenient to exploit an algorithm of the quasi-Newton class. Obviously, the gradient must be available either in analytical or numerical form. This second option typically burdens even more the calculation, since it requires a repeated functional evaluation. In this sense, exploiting the expertise drawn from the computational world becomes crucial to make the method practically feasible for electrically large antennas, showing how the two worlds of measurements and computation can profit of each other to produce unprecedented results.

With particular reference to this paper, we show which beneficial effects an optimization algorithm based on the analytical evaluation of the gradient can achieve in terms of execution time. The case of aperture antennas is here dealt with, in the planar scanning geometry, wherein probe compensation is explicitly considered.

II. THE NFFF TRANSFORMATION

Let us consider an aperture AUT having a $2a_{ap}x2b_{ap}$ sized rectangular effective aperture $\mathcal{A}$, centered in x-y plane of the Oxyz reference system (see Fig. 1), and let us denote with $\underline{E}_a$ the aperture field (tangential components). Furthermore, let us assume that the samples of the field radiated by the AUT are collected over a planar surface $\mathcal{D}$ bounded by a 2ax2b sized rectangle, located at a distance z_0 from $\mathcal{A}$. The parameters a and b are defined according to dimensions of the available scanning system.

The method calculates the FFP given $\underline{E}_a$. This, in turn, is determined starting from the measured field on $\mathcal{D}$, by solving a linear inverse problem, defined by a linear operator, say $\mathcal{T}$, mapping $\underline{E}_a$ onto the measured voltages V on $\mathcal{D}$. The numerical inversion of $\mathcal{T}$ requires its discrete counterpart, determined by considering the smallest finite dimensional functional subspace containing

Submitted On: February 2, 2016
Accepted On: May 7, 2016

the relevant functional component of $\underline{E}_a$. After this, discretization is obtained by:

- Expanding Ea by means of an orthonormal basis of the functional subspace above [2-4];
- Considering the measured voltages Vm at the M sampling points, whose coordinates are (xm,ym,z0);

And so the problem turns into its algebraic counterpart, which can be written as:

$$\underline{Y} = \underline{\underline{T}}\,\underline{X}, \quad (1)$$

where $\underline{Y}$ is the vector containing the measured voltages, $\underline{X}$ is the vector containing the unknown expansion coefficients of $\underline{E}_a$, and $\underline{\underline{T}}$ is the matrix representing the discrete counterpart of the operator $\mathcal{T}$. To calculate $\underline{E}_a$ is equivalent to determine $\underline{X}$ from $\underline{Y}$ by solving the linear system in Eq. (1). Obviously a regularization strategy is needed to circumvent the ill-conditioning of $\underline{\underline{T}}$. In the following Eq. (1) will be detailed for the case of a scalar problem, with a linearly polarized aperture field $\underline{E}_a=E_a\hat{\imath}_y$, and standard open-ended waveguide (OEWG) probe, assumed to be linearly polarized and oriented along $\hat{\imath}_y$, assuming negligible the x-component of the probe response.

Accordingly, the voltage V_m measured at the m-th measurement point (x_m,y_m,z_0) can be written as [2,3]:

$$V_m = \frac{1}{z_0}\int_{-a_{ap}}^{a_{ap}}\int_{-b_{ap}}^{b_{ap}} l(x_m,y_m,x',y')h_y E_a dx'dy', \quad (2)$$

where $\beta=2\pi/\lambda$, λ being the wavelength, $l(x,y,x',y')=g(y,y')f(R)$ where $g=g(y,y')=[z_0^2+(y-y')^2]$, R is given by:

$$R = \sqrt{(x-x')^2+(y-y')^2+z_0}, \quad (3)$$

and

$$f(R) = \frac{1}{2\pi}\left(\frac{j\beta}{R}+\frac{1}{R^2}\right)\frac{e^{-i\beta R}}{R}, \quad (4)$$

and $h_y= h_y(x,y,x',y')$ is the y-component of the probe response, in the reference system Oxyz, and $E_a=E_a(x',y')$. Regarding E_a, as in [2,3] it is expanded by using the visible Prolate Spheroidal Wave Functions (PSWF) [8], so to take into account for the geometry of the aperture and for the obvious assumption of non-superdirective source. In this way, E_a is written as:

$$E_a(x,y) = \sum_{p=1}^{P}\sum_{q=1}^{Q}\alpha_{pq}\Lambda_p(c_x,x)\Lambda_q(c_y,y), \quad (5)$$

where $\Lambda_i[c_w,w]$ is the i-th, 1D PSWF with "space-bandwidth product" c_w [8], $c_x=a_{ap}u'$, $c_y=b_{ap}v'$ and u' and v' locate the spectral region of interest [8], as $u'\leq\beta$ and $v'\leq\beta$, $P=Int[4a_{ap}/\lambda]$ and $Q=Int[4b_{ap}/\lambda]$, Int[•] denoting the integer part of its argument.

Accordingly, $\underline{X}$ is a vector of S=PQ elements containing the expansion coefficients $\alpha_{p(s)q(s)}$, where p(s) and q(s) map the index s into the corresponding PSWF indices p and q, while $\underline{\underline{T}}$ is an MxS matrix whose entries are given by:

$$\frac{1}{z_0}\int_{-a_{ap}}^{a_{ap}}\int_{-b_{ap}}^{b_{ap}} l h_y \Lambda_{p(s)}(c_x,x')\Lambda_{q(s)}(c_y,y')dx'dy', \quad (6)$$

where both l and h_y are evaluated at the m-th observation point (x_m,y_m).

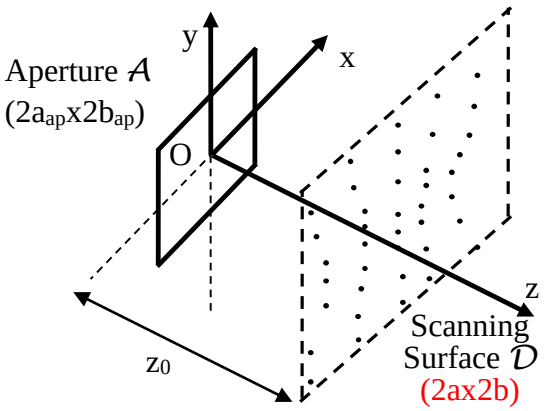

Fig. 1. Geometry of the problem.

III. GRADIENT-BASED OPTIMIZATION PROCEDURE

The DFS and M are obtained via a SVB optimization, according to the procedure in [2,3] based on the maximization of the functional:

$$\Xi = \sum_{k=1}^{K}\frac{\sigma_k}{\sigma_1}, \quad (7)$$

where σ_k are the K singular values of the matrix $\underline{\underline{T}}$, ordered in decreasing order. As shown in [2,3], to keep low the number of unknowns, it is convenient to adopt a proper representation of the measurement point locations. In particular, the sampling points can be determined by starting from an auxiliary uniform Cartesian grid (ξ_m,η_m) by means of a couple of "distortion" mappings, say w_x and w_y, to be determined. Accordingly:

$$\begin{cases} x_m = w_x(\xi_m,\eta_m) \\ y_m = w_y(\xi_m,\eta_m) \end{cases}, \quad (8)$$

where w_x and w_y are represented by means of W basis functions (e.g., polynomials), say τ^x and τ^y, respectively:

$$\begin{cases} w_x(\xi_m,\eta_m) = \sum_{r=1}^{W}\chi_r\,\tau_r^x(\xi_m,\eta_m) \\ w_y(\xi_m,\eta_m) = \sum_{r=1}^{W}\chi_{r+W}\,\tau_r^y(\xi_m,\eta_m) \end{cases}. \quad (9)$$

And so, for a given M, the unknowns turn to be the coefficients χ_r, and the measurement points are determined as the ones maximizing Ξ. The effective and efficient maximization of Ξ is crucial to make the procedure successful.

Among the quasi-Newton class local tools, a very widespread choice if the the Broyden-Fletcher-Goldfarb-Shanno (BFGS) scheme [9]. Given a function $f(\underline{x})$ to be optimized, where $\underline{x}$ is the vector of the unknown parameters, the solution at each iteration is obtained by exploiting the expression of the gradient ∇f and an approximate inverse of the Hessian matrix $\underline{\underline{H}}$, obtained by an update formula based on the f and ∇f evaluation at the current and preceding iteration. Two options are available. The first estimates ∇f numerically and can be very time consuming, especially for large problems and

computationally burdened f. The second analytically evaluates ∇f and typically gives better results in terms of accuracy and computational complexity being often comparable to that of a single evaluation of f [10], since, in our case, the analytical expression of the gradient is at disposal.

In the case of interest, the analytical evaluation of ∇f requires the evaluation of the partial derivatives of Ξ, and then those of σ_k, with respect to the χ_r's. The derivative of interest can be written as [11]:

$$\frac{\partial \sigma_k}{\partial \chi_r} = \frac{1}{2\sigma_k}\left[\underline{u}_k^H \left(\frac{\partial \underline{\underline{T}}}{\partial \chi_r}\underline{\underline{T}}^H + \underline{\underline{T}}\left(\frac{\partial \underline{\underline{T}}}{\partial \chi_r}\right)^H\right)\underline{u}_k\right], \qquad (10)$$

where $\underline{u}_k$ is the k-th left singular vector of the matrix $\underline{\underline{T}}$, respectively, while $\partial\underline{\underline{T}}/\partial\chi_r$ denotes a matrix whose entries are the derivatives of the entries of $\underline{\underline{T}}$, shown in Eq. (6), with respect to the χ_r's, which in turn involve the derivatives of the points coordinates with respect to the χ_r's, and the apex H stands for Hermitian. Regarding the computational point of view, for the considered test cases, the calculation of Eq. (10) is mainly burdened by the term $\partial\underline{\underline{T}}/\partial\chi_r$. Anyway, the evaluation time can be reduced by recasting Eq. (10) to calculate simultaneously all the derivatives, using the optimized matrix-matrix multiplications [12], as:

$$\frac{\underline{\underline{\rho}}}{2} .* diag\left[\underline{\underline{U}}^H \left(\frac{\partial \underline{\underline{T}}}{\partial \chi_r}\underline{\underline{T}}^H + \underline{\underline{T}}\left(\frac{\partial \underline{\underline{T}}}{\partial \chi_r}\right)^H\right)\underline{\underline{U}}\right], \qquad (11)$$

where $\underline{\underline{U}}$ is the matrix of the left singular vectors, *diag* provides the diagonal entries of the argument, the symbol .* represent the element-wise multiplication, and $\underline{\rho}$ is a vector such that $\rho_k=1/\sigma_k$. In particular the entries of $\partial\underline{\underline{T}}/\partial\chi_r$ are given by:

$$\frac{1}{z_0}\int_{-a_{ap}}^{a_{ap}}\int_{-b_{ap}}^{b_{ap}}\left[g\left(\frac{\partial f}{\partial \chi_r}h_y + \frac{\partial h_y}{\partial \chi_r}f\right) + \frac{\partial g}{\partial \chi_r}f h_y\right]\Lambda_{p(s)}(c_x, x')\,\Lambda_{q(s)}(c_y, y')dx'dy', \qquad (12)$$

where f, g, h_y and the corresponding derivatives are evaluated at the m-th observation point, and

$$\frac{\partial f(R)}{\partial \chi_r} = \begin{cases} \frac{t(R)(x-x')}{R}\tau_r^x(\xi,\eta) & \text{for } 1\le r\le W \\ \frac{t(R)(y-y')}{R}\tau_r^y(\xi,\eta) & \text{for } W+1\le r\le 2W \end{cases}, \qquad (13)$$

with

$$t(R) = \frac{1}{2\pi}\left(-3j\beta - \frac{3}{R} + \beta^2 R\right)\frac{e^{-i\beta R}}{R^3}, \qquad (14)$$

and

$$\frac{\partial g}{\partial \chi_r} = \begin{cases} 0 & \text{for } 1\le r\le W \\ 2(y-y')\tau_r^y(\xi,\eta) & \text{for } W+1\le r\le 2W \end{cases}, \qquad (15)$$

while the term $\partial h_y/\partial\chi_r$ depends on the peculiar choice for h_y and is here omitted for just the sake of brevity.

IV. RESULTS

A numerical analysis has been carried by performing the optimization of Ξ, by using both the numerical and the analytical evaluation of the gradient, for antennas with different sizes and a fixed aspect ratio $a_{ap}/b_{ap}=5/3$. In particular, Case A, B and C refer to antennas with $2a_{ap}=5\lambda$, $2a_{ap}=10\lambda$ and $2a_{ap}=15\lambda$, respectively. For each case, as mentioned before (for a deeper discussion see [2,3]), Ξ has been optimized for different values of M, using the solution obtained at the previous step as starting point of the current one. In particular, by assuming $M=N_xN_y$, the values for M are here obtained by progressively increasing N_y, and using $N_x/N_y=5/3$, according to the aspect ratio of $\mathcal{A}$. The results are reported in Table1 wherein, for each value of N_y, the number of iterations (#it), the execution time and the optimal values of Ξ are shown. By labeling as t_N and t_A the execution times associated to the numerical and analytical case, respectively, the corresponding speedup $S=t_N/t_A$ has been calculated for each value of N_y. Also, the whole speedup S_C for each case is shown. The tests have been performed by using a compiled Matlab script on a PC with an Intel I7-4712HQ CPU working at 2.3 GHz and 16 GB RAM. It's worth noting that, regarding the numerical evaluation of the gradient, different approaches can be adopted [13]. Here the forward finite difference scheme is adopted, the "fastest possible" derivative approximation. The results in Table 1 show that the approach based on the analytical expression of the gradient leads to a faster functional minimization even with respect to the fastest numerical evaluation of the gradient. Furthermore, as it can be noted, S_C remains about constant, even if the aperture area in the biggest case is increased of a factor 9 with respect to the smaller antenna. The behavior is justified by the equal number of expansion coefficients (gradient components) adopted in Eq. (9), 2W, which remains the same across all the test cases. Obviously, since the computing time grows with the antenna size, the faster calculation turns remarkable for larger antennas. Finally, the approach has been exploited for the experimental characterization of standard gain horn Narda 640, at the working frequency of 8 GHz, taking into account also for the probe effects as discussed above. The effective aperture parameters are a_{ap}=4.9 cm and b_{ap}=3.9 cm, while the measurements have been collected on a planar region with z_0=37.5 cm.

A standard OEWG working in the X band has been used as probe. The measurements have been carried out within the anechoic chamber available at the Dipartimento di Ingegneria Elettrica e delle Tecnologie dell'Informazione, Università di Napoli Federico II. In particular, two sets of measurements have been acquired, one for the optimized scanning and the other for the standard sampling, to perform a comparison. The characterization with the standard sampling has required about 5265 samples ($\lambda/2$ sampling rate), while the number of samples obtained with the proposed technique is equal to 130 (with P=6, Q=5). In Fig. 2 the DFS is reported, while in Fig. 3 the reconstructed FFP is presented (blue cross) together with the one obtained with the standard sampling (red lines), for v=0 and u=0, respectively ($u=\beta\sin\theta\cos\varphi$, $v=\beta\sin\theta\sin\varphi$). A satisfactory agreement is

obtained.

Table 1: Optimizer performance for the case of numerical and analytical gradient evaluation

		Numerical Grad			Analitical Grad				
	Ny	#it	t_N	Ξ	#it	t_A	Ξ	S	S_C
Case A	6	14	13,8	25,4	28	10,3	25,4	1,3	1,7
	8	12	5,4	34,3	5	3,5	34,3	1,5	
	10	14	10,2	38,2	4	4,9	38,2	2,1	
	12	16	15,6	40,6	8	12,6	40,6	1,2	
Case B	12	5	194,4	110,8	30	230,9	107,7	0,8	2
	14	6	330,9	123,1	11	132,7	122,9	2,5	
	16	5	343,7	133,7	9	150,4	133,8	2,3	
	18	21	641,6	140,9	9	185,0	140,8	3,5	
Case C	19	4	2086,0	246,2	20	1698,1	249,8	1,2	2
	21	40	3574,6	281,7	14	1410,1	273,9	2,5	
	23	5	2085,2	295,8	11	1370,1	292,5	1,5	
	25	5	5460,9	308,0	9	1417,3	306,5	3,9	

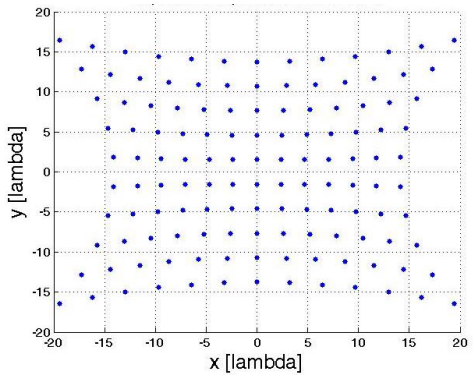

Fig. 2. The locations for the measurement points.

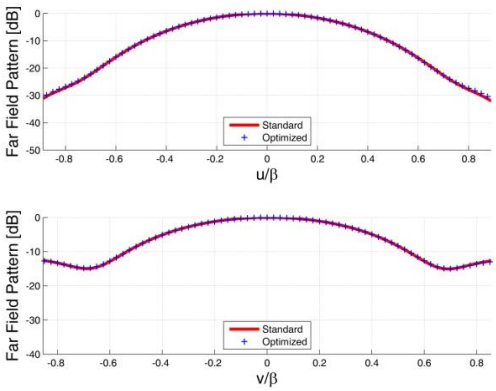

Fig. 3. Cut of the FFP along the u and v axis reconstructed with standard sampling (red line) and with optimized approach (blue cross).

V. CONCLUSIONS

The use of the analytical expression of the gradient evaluation in the optimized NF characterization has been adopted to speed-up the SVB optimization. The analysis show remarkable improvements in terms of computing time when comparing the proposed approach with the one based on the numerical evaluation of the gradient.

REFERENCES

[1] A. D. Yaghjian, "An overview of near field antenna measurements," *IEEE Trans. on Antennas and Propagation*, vol. 34, no. 1, pp. 30-45, 1986.

[2] A. Capozzoli, et al., "Singular value optimization in plane-polar near-field antenna characterization," *IEEE Antennas Prop. Mag.*, vol. 52, no. 2, pp. 103-112, Apr. 2010.

[3] A. Capozzoli, et al., "Field sampling and field reconstruction: a new perspective," *Radio Sci.*, vol. 45, RS6004, pp. 31, 2010.

[4] A. Capozzoli, et al., "NUFFT-accelerated plane-polar (also phaseless) near-field/far-field trans-formation," *Progress In Electromagnetics Research M*, vol. 27, pp. 59-73, 2012.

[5] A. Capozzoli, et al., "Photonic probes and advanced (also phaseless) near-field far-field techniques," *IEEE Antennas Prop. Mag.*, vol. 52, no. 5, pp. 232-241, Oct. 2010.

[6] A. Capozzoli, et al., "Multi-frequency planar near-field scanning by means of SVD optimization," *IEEE Antennas Prop. Mag.*, vol. 53, no. 6, pp. 212-221, Dec. 2011.

[7] A. Capozzoli, et al., "A probe compensated helicoidal NF-FF transformation for aperture antennas using a prolate spheroidal expansion," *Int. J. of Antennas Prop.*, vol. 2012, 2012.

[8] H. J. Landau and H. O. Pollak, "Prolate spheroidal wave functions, Fourier analysis and uncertainty – III: the dimension of essentially time- and band-limited signals," *Bell Syst. Tech. J.*, vol. 41, pp. 1295-1336, 1962.

[9] W. H. Press, et al., *Numerical Recipes in Fortran 77: The Art of Scientific Computing*, Cambridge University Press, 1992.

[10] Matlab User's Manual, http://it.mathworks.com/help/optim/ug/when-the-solver-might-have-succeeded.html

[11] G. H. Golub and C. F. Van Loan, *Matrix Computations*, Baltimore, John Hopkins University Press, 1996.

[12] K. Atkinson and D. D. K. Chien, "A fast matrix-vector multiplication method for solving the radiosity equation," *Adv. in Comput. Math.*, vol. 12, no. 2-3, pp. 151-174, Feb. 2000.

[13] N. S. Bakhvalov, *Numerical Methods*, Mir Publishers, Moscow, 1977.